Voyager RADVS-Exhaust Plume Interference

J. F. Cashen
Hughes Aircraft Company, Space Systems Division

J. G. Seubold
Hughes Aircraft Company, Space Systems Division

R. R. Gold
Hughes Aircraft Company, Space Systems Division

VOYAGER RADVS-EXHAUST PLUME INTERFERENCE

J. F. Cashen, * J. G. Seubold, * R. R. Gold**
Hughes Aircraft Company, Space Systems Division
El Segundo, California

Summary

It is generally accepted that there is virtually no interference between the Surveyor and Apollo LM rocket exhaust plumes and their respective RADVS systems. The obvious tendency to extrapolate the conditions of the Surveyor and Apollo LM vehicle to Voyager would lead to the similar conclusion that no interference problem should exist. However, preliminary calculations on several proposed Voyager descent engines indicate that severe interference with the radar may occur. The essential difference in this case is the back pressure of the Martian atmosphere which confines the plume and introduces shock and mixing layer regions and the associated high gas and electron densities. The extent of the problem was sufficiently serious to impose a major constraint on the preliminary Voyager design.

Figure 1(a) shows conceptually the Voyager entry and the RADVS controlled soft landing, and Figure 1(b) shows two candidate RADVS systems. Only the Surveyor type was studied, however the results are equally valid for either system.

I. Background

A. Plume Interference in Other RADVS*** Systems

Prior to the SC-1 mission, JPL predicted that Surveyor would not experience plume-RADVS interference.[1] Telemetry returns from that and subsequent missions verify this result. Although the RADVS beams intersect the plume, high electron concentrations associated with a confined plume and shock regions are precluded as a result of expanding into a vacuum. This will be examined in more detail in the next section. The T-2 series balloon drop tests (designed to verify the Surveyor spacecraft soft landing capabilities) revealed no interference of any form[2] despite the atmospheric back pressure and resultant shock structure. An analysis of the flowfield and RADVS beam location indicates in a simple geometric manner how this conclusion is reached (see Figure 2). An insight into the Voyager problem is also revealed on the same basis.

Since the Surveyor engines were designed to work in a vacuum environment, the atmospheric T-2 tests required a modification. The expansion ratio of the nozzle was reduced so that the engines would not be overexpanded. This modification reduced the nozzle radius from 2 1/2 inches to 1/2 inch. Further, the plume does not freely expand as in the vacuum case, but is restricted by the atmospheric back pressure on the exhaust flow, as determined by the ratio of exit pressure to atmospheric pressure. Figure 2 shows the skewed -3 db ray line of doppler beam number 2‡ in the cylindrical coordinate system of the number 1 vernier engine plume which is gimbaled towards the beam‡‡ (the straight ray line appears curved because of this projection). This particular beam-plume geometry affords the closest proximity. It is apparent that the radar beam misses the T-2 plume by a substantial margin. Regions of high electron concentration are so inaccessible that no interference of any form is possible.

Also shown is the plume boundary for the actual Surveyor mission (from the JPL analysis). Even though the beam intersects the plume, no interference was predicted or observed due to the aforementioned absence of high electron concentration with a vacuum ambient.

An analysis similar to JPL's was carried out by AeroChem[3] with regard to the Apollo LM RADVS-plume interference problem. They likewise came to the conclusion that there would be no serious interference. However, they did indicate that the safety margin was less than it had been with Surveyor. The Langley Research Center later verified these calculations with an experiment.

II. Voyager Vernier Lander Systems

Two independent lander systems have been studied. These are detailed in Table 1.

---

*Member of Technical Staff, Aerospace Physics Research Department.

**Manager, Aerospace Physics Research Department.

***Radar altitude and doppler velocity sensor.

‡A -3 db ray is defined as a ray following a path which is 3 db below the peak beam intensity. It is parallel to the peak intensity ray in the near field and skewed at the beam half angle in the far field.

‡‡The number 1 vernier engine has the capability of 5.5 degree gimbaling.

Table 1

Lander System	Number of Verniers	Engine Location (From Vehicle C/L)	Maximum Thrust (Per Engine)	Exit Diameter	Fuel
A	3	42-inch radius	1500 pounds	10.2 inches	N_2O_4/MMH*
B	6	54-inch radius	1000 pounds	8.5 inches	MMH

*Mono-methyl hydrazine.

The principal difference between the two systems aside from the number of engines is the fuel. The monopropellant of system B produces chamber temperatures about half that of the bipropellant of A resulting in electron density levels several orders of magnitude lower.

The RADVS is only used during the terminal portion of the Voyager landing. The maximum altitude of interest is still sufficiently low so that the ambient pressure differs only slightly from the surface pressure. The present estimate of Martian surface pressure is a lower bound of 5 millibars (NASA model VM-8) and an upper bound of 20 millibars (NASA model VM-10). Both these models have been considered in this study.

Spectroscopic studies of Mars indicate that the planet's atmosphere is devoid of oxygen as gas, best estimates being that it is predominately CO_2. This is an important point when considering plume interference, since electron-producing afterburning of residual fuel in the plume cannot occur as it does in earth's atmosphere.

III. Plume Properties

The important gasdynamic features of the near field rocket plume are shown in Figure 3. It is interesting to note that 3(a) shows the conditions for the largest Voyager plume (full thrust in a VM-8 atmosphere), and the plume is still very much confined. If the jet exit pressure p_e is greater than the ambient pressure p_a, the jet expands toward ambient pressure. There is a tendency to overexpand, so that the pressure along the centerline actually goes below the ambient pressure. This causes oblique and normal shocks to be formed in the process of equilibrating the ambient and jet pressures. Along the boundary of the plume the exhaust gas mixes in turbulent flow with the atmosphere.

Plume analysis starts with a method of characteristics calculation for the inviscid flow. This gives the boundary without mixing, the oblique shock location, and all the gasdynamic properties. It does not tell where the normal shock appears, which must be determined by empirical correlation. The mixing layer is calculated by superposition along the inviscid boundary. Due to freezing in the nozzle of the exhaust mixture with respect to ionization/recombination, the ionization reactions in the plume can be neglected (except for the normal shock regions). Once the level of freezing has been established the electron densities depend only on the density of gas in the plume. After the normal shock, the high temperature is assumed to produce equilibrium again. Downstream of the normal shock the gasdynamics becomes more complicated and little analysis is possible at this time although some rough estimates of rate of growth of the plume and the location of additional normal shocks in this region are included.

A. Method of Characteristics

The method of characteristics is a reliable and generally accepted method of determining gasdynamic flow properties in inviscid, supersonic flow. It does not give any information on the location of the normal shock, which will be discussed in the following section, and indeed keeps on calculating past the location of the normal shock. The flow behind the shock is, of course, subsonic, and the method of characteristics is no longer applicable. It is this combination of subsonic core surrounded by supersonic flow surrounded by subsonic flow, with the accompanying mixing layers, that makes analysis impossible.

Figure 3 shows the inviscid boundary and oblique shock boundary predicted by the method of characteristics. The method also provides necessary information to predict the mixing layer and the normal shock diameter. The primary parameter in determining these profiles (for a given nozzle) is the ratio of ambient to nozzle exit pressure, p_a/p_e; the higher this ratio, the more confined the plume.

B. Normal Shock Regions

The location of the normal shock is determined by the empirical relation

$$\frac{x_g}{d_e} = 0.69\, M_e \left(\frac{\gamma\, p_e}{p_a}\right)^{1/2} \qquad (1)$$

where x_g = distance to normal shock, d_e = nozzle exit diameter, M_e = nozzle exit Mach number, p_e = nozzle exit pressure, γ = specific heat ratio, and p_a = ambient pressure. This correlation is due to Lewis and Carlson,[4] and checks well with other experiments and analyses. Normal shock locations (for System A) as functions of thrust for two Martian atmospheric pressures are shown in Figure 4(a). The diameter of the normal shock is determined by its intersection with the oblique shock, as determined from the method of characteristics. For small p_e/p_a there may be no normal shock at all; we may consider that the equation still applies but the diameter of the normal shock is zero.

The normal shock locations for maximum thrust also appear in the complete plume description of Figure 3. The radius and location of first normal shocks for different thrust levels and ambient pressures is shown in Figure 4(b) for System A. For the range of p_e/p_a under consideration, the parameter p_e/p_a determines both shock location and size, so one curve covers both the VM-8 and VM-10 atmospheres. Approximately, when the nozzle is ideally expanded ($p_e/p_a = 1$) the normal shock is about 25 inches downstream.

The conditions behind the normal shock can be found from the gas state just ahead of the shock (as given by the method of characteristics). Labeling the conditions just upstream with a subscript 1, and downstream with a subscript 2, we then have the following relations for calculating conditions downstream of the normal shock:

$$p_1 = \frac{P_1}{p_e} p_e = \left[\frac{1 + \frac{\gamma - 1}{2} M_e^2}{1 + \frac{\gamma - 1}{2} M_1^2} \right]^{\gamma/\gamma - 1} p_e \qquad (2)$$

$$\frac{p_2 - p_1}{p_1} = \frac{\gamma + 1}{2\gamma} \left(M_1^2 - 1 \right) \qquad (3)$$

The change in γ going through the normal shock has been neglected. For System A at full thrust we then have $p_2 = 0.926$ psi for the VM-10 atmosphere and $p_2 = 0.28$ psi for the VM-8 atmosphere. Note that these are 3 to 4 times atmospheric pressure. The temperature T_2 is assumed to be equal to chamber temperature: $T_2 = 3390°K = 6100°R$. This is a good approximation as the electron density is only very weakly a function of T_2 anyway.

Behind the normal shock the temperature is sufficiently high and the gas velocity sufficiently low to produce equilibrium ionization. For a given pressure the equilibrium electron density is almost independent of temperature in the temperature range of interest. Thus any errors in temperature are unimportant. Any errors in the calculated gas pressure will be fractional, and can change the electron density only by a corresponding fraction.

Collision frequency predictions were based upon standard methods. The H_2O exhaust product is the largest contributor to the collision frequency, having a very large collision cross section. [5]

For the present application the thickness of uniform conditions behind the shock was taken to be one-half the shock diameter. We can be sure that within one diameter, gasdynamic expansion will significantly accelerate and cool the gas, so that in equilibrium the electron density is reduced. RF interference downstream of this uniform shock layer may not be negligible, but at this time we do not have the capability of calculating it.

The important parameters for normal shock interference with the engines at full thrust are shown in Table 2.

The impurity level expected in the System A fuel was undetermined at the time of the analysis. Previous studies of bipropellants indicated a minimum of 1 PPM and a practical maximum of about 10 PPM. The System B monopropellant was not expected to have over 3 PPM impurities. The whole question of impurities is dependent to a great extent upon handling and a specific prediction is difficult to make.

If it were possible to reduce the impurity level to zero, chemical concentration effects would still create some electrons. The electron density produced by this mechanism is estimated to be the equivalent of that generated by a Na impurity of 0.5 PPM. Thus, reduction of the impurity concentration has only limited effectiveness.

As most of the gas does not pass through the first normal shock, the supersonic flow surrounding the normal shock can mix with the core of the subsonic flow, accelerate it back into the supersonic range, and produce another normal shock. In most cases there are no more than three or four normal shocks, although more have been observed in isolated cases. The additional normal shocks will be smaller than the first one, and the pressure behind them will be lower, probably close to ambient. The length of a "cell," i.e., the distance between shocks, is fairly constant, except that the first cell, from nozzle exit to first normal shock, is somewhat shorter.

C. Mixing Region

Along the boundary between the inviscid jet flow and the outside air, a mixing layer forms. This is the second major factor that does not exist at all in a vacuum expansion. Fortunately for Voyager, the Mars atmosphere does not contain oxygen, so the fuel-rich exhaust cannot burn in the mixing layer.

Properties in the mixing layer can be calculated using the method developed by Seubold. [6] Results of this calculation are shown in Figure 5 (for System A at maximum thrust). The temperature ratio $\tau = T/T_{jet}$ is based on an expanded jet temperature of $1054°R$. Due to recovery of kinetic energy in the mixing layer, the peak temperature is about $2000°R$. The velocity ratio u/u_g is self-explanatory. The mass fraction of gas at any point that came from the exhaust is F'. The normalized ordinate $\eta = \varphi - \varphi_n / \varphi_j - \varphi_n$ where $\varphi_j = 0.73$, $\varphi_h = 3.20$ (results of the calculation), are the extremes of φ on the freestream flow and jet sides, respectively, and $\varphi = \sigma y/x$ where x is the running length along the jet boundary and y the perpendicular. The spreading parameter σ is an empirical number which is a measure of the turbulent viscosity. We have taken $\sigma = 19$, which appears to be a good number for most rocket exhausts in an ambient atmosphere.

The mixing layer analysis described here is limited to the two-dimensional problem, and for this reason will no longer be applicable much beyond the normal shock. This is no particular handicap, as we cannot compute core conditions downstream of the normal shock region anyway.

Table 2

	System A				System B
	VM-8		VM-10		VM-10
	1 PPM	10 PPM	1 PPM	10 PPM	3 PPM
p_2 (psi)	0.28		0.926		2.5
Shock diameter (inches)	8.2		27		10
Shock layer thickness (inches)	4		13		5
Collision frequency (collisions/sec)	0.375×10^{10}		0.124×10^{11}		3.1×10^{10}
Electron density, (cc^{-1})	0.45×10^{11}	4.5×10^{11}	1.4×10^{11}	1.3×10^{12}	3×10^{5}

Application of this mixing layer analysis to calculation of electron densities and collision frequencies is described in the next section.

D. Ionization Outside of Normal Shock Regions

Although the ionization is by far the highest behind the normal shock, electron densities elsewhere in the plume are not necessarily negligible. The temperatures to be considered are quite low, even in the mixing layer and after oblique shocks, so that the ionization/recombination reactions may be taken to be frozen. We have then only to determine exit plane ionization and scale according to gas density.

Reference 3 states freezing with respect to ionization produces an actual exit electron density about half that if the flow were frozen in the chamber. However, Smoot[7] has made measurements which showed the factor to be 1/10 or less. We have chosen to use the latter so that

$$(N_e)_{plume} = \frac{(N_e)_{chamber}}{10} \frac{(\rho)_{exhaust}}{(\rho)_{chamber}} \qquad (4)$$

where the subscript "exhaust" refers to the gas coming out the nozzle, and "plume" includes mixing with the atmosphere, if any.

E. Middle and Far Field Effects

After the first normal shock, the above gasdynamic analytical methods break down, due to the complex combination of subsonic and supersonic flows and multiple mixing layers. In the far field, where all the flow is subsonic, some empirical correlations are possible for the present case, where no afterburning takes place. In the middle region no meaningful calculations can be made, but some educated qualitative comments are possible. In this section we will discuss some of the middle and far field effects as far as presently available technology allows.

1. Coalescence of Jets. All of the analysis described in this paper concerns the plume from a single nozzle. In this section we will explain quantitatively why we do not need to worry greatly about effects from combined jets.

Consider System A at full thrust in the VM-8 atmosphere. This is the case of maximum plume expansion. A schematic of the key features is shown in Figure 6(a). The minimum radius of the engine location from the center of the vehicle is 42 inches, which means the engines are 72.6 inches apart. The initial expansion of the plume takes the inviscid boundary out to a radius of about 22 inches, and the mixing layer to 38 inches, so some intermixing of plumes will take place. However, this is only in the cool outer regions of the mixing layer. The inner portion of the plume is overexpanded at this axial station, and will adjust to the ambient pressure. We should then consider as a basic inviscid radius not the 22 inches of the maximum expansion, but 12.3 inches corresponding to an ideal expansion to ambient pressure. If we do this and use the 2-D boundary layer spreading rate as calculated in the previous section, the mixing layers of the plume begin to coalesce 142 inches downstream of the exit, i.e., significantly beyond the first normal shock. Not until much further downstream, at about 250 to 300 inches, has the mixing progressed far enough to cause coalescence of regions of high temperature and high electron densities. By this time the mixing is also attacking the jet cores, reducing both temperature and velocity, so the actual conditions are much less severe than suggested by extension of the two-dimensional analysis. Thus it is reasonable to say that, even in this extreme case of the lowest atmospheric pressure and minimum engine spacing, the engines are sufficiently far apart that coalescence of the plumes involves only the cooler gases of the mixing layer, and can thus be neglected with regard to electron concentrations and the attendant RF interference.

Although the System B engines are closer together, their plumes are considerably smaller. The result is that the coalescence has approximately the same description as above, and the same conclusion about interference can be inferred.

2. Opposing Flow. At the initial firing of the Voyager verniers the vehicle is still descending at a high velocity, and the influence of the opposing flow could possibly affect the plume. A rough way of looking at this would be to compare

the maximum vehicle velocity of about 1000 fps to the jet velocity of about 10,000 fps. If we want to be more sophisticated, we try to compare stagnation pressures in the plume and atmospheric flow. Take the formula for stagnation pressure

$$P_{stag} = P_{static} \left(1 + \frac{\gamma - 1}{2} M^2\right)^{\gamma/\gamma-1} \qquad (5)$$

and assume the specific heat ratio γ of the jet is about that of the atmosphere, which is reasonable considering a lot of mixing of the plume with the atmosphere will take place before the exhaust flow is reversed. The proposed flight paths all involve starting the engines at less than M = 1. Thus the stagnation pressure in the plume is above the stagnation pressure of the opposing flow at the end of the supersonic core, where M = 1. A plot of supersonic core length as a function of thrust for System A for two atmospheric pressures is shown in Figure 6(b). The calculations were based on the method of Reference 8 (Shirie and Seubold). This may be compared with the normal shock location shown previously in Figure 4(a). By the end of the supersonic core, mixing of the plume with the air has reduced the plume temperature drastically, and the time for the gas to get to this position is sufficiently long that some recombination reaction will have taken place. Further, even if the flow were completely frozen, only a fraction of the plume at this point came out of the engine, the rest consisting of mixed atmosphere, so the electron densities can only be a fraction of what they were in the first cell. For the same reasons, we neglect the combined effects of coalescence of multiple plumes and opposing flow.

From the above argument we conclude that the portion of the plume in which high electron concentrations are found is not subject to serious changes due to opposing flow. The influence of the downstream portion of the plume blowing back around the upstream portion has not been considered, but is believed to be a higher order effect.

IV. RF Interference

Once the plume is defined, as in Section III, then the next task is the estimation of interference. There are four types of interference possible. They are, in probable order of importance:

1. Attenuation
2. Refraction
3. Reflection
4. Phase shift

All can be predicted theoretically using the results of gasdynamic and chemical kinetic analyses such as described in Section III and the established techniques of the WKB approximation to the Helmholtz equation and geometric optics.

All four of the above interference mechanisms have noise perturbations about their steady state values. Although the most severe interference is generally due to the steady state effects, the noise can in itself cause significant interference to the operation of a CW doppler radar such as RADVS.

The interference listed above is caused by the interaction of the radar's electromagnetic wave and the electrons in the flame plasma of the plume. The plasma can be described, electromagnetically, by its complex dielectric constant

$$K = 1 - (f_p/f)^2/(1 - j\,\nu_c/2\pi f) \qquad (6)$$

where

$f_p = 9 \times 10^3 N_e^{1/2}$ (cps)

N_e = electron density (cc^{-1})

f = signal frequency (cps)

ν_c = electron-neutral particle collision frequency (sec^{-1})

The plume's index of refraction is then given by

$$n^*(r) = K(r)^{1/2} \qquad (7)$$

where, in general, it is a variable of position (r).

Plasma absorption is given, for many plume applications by the WKB approximation of the wave equation, as

$$A(db) = 8.68 \frac{2\pi f}{c} \int_0^L \mathrm{Imag}\{n^*(r)\}\,dr \qquad (8)$$

where c = speed of light (3×10^{10} cm sec^{-1}) and L is the total path (cm).

Total refraction is found from considering the incremental local refraction of a three-dimensionally inhomogeneous refractive medium. Analysis of this is quite tedious and requires machine computation. The plasma parameter of importance for this effect is the real part of n*(r) or more specifically its gradient.

Reflection is also a function of the gradient of a real part of n*(r), the degree being proportional to the dimensions and size of the gradient relative to the free space wavelength of the e.m. wave. In the limit of infinite gradient the well known Fresnel reflection laws of optics apply. The internal shocks present in the Voyager plume are sharp enough, relative to the RADVS wavelength, so that the infinite gradient approximation applies.

Phase shift also depends upon the real part of n*(r). The relative phase shift, compared to that in the free atmosphere, is given by

$$\Delta\varphi(\mathrm{rad.}) = \frac{2\pi f}{C} \left(n_a L - \int_0^L R_e\{n^*(r)\}\,dr \right) \qquad (9)$$

where n_a is atmospheric index.

If the plume is "cool enough" so that the electron concentration is low, then the plume index of refraction is that of the hot plume gases. This can differ enough from the free atmospheric index to cause small amounts of refraction, phase shift and, most significantly for RADVS, reflection. Although not previously considered in plume studies, it provides a limiting index value and in certain situations can cause important interference.

The interference levels experienced in each of the various plume regimes are assessed in the following:

A. Normal Shock

This region of the plume provides the most severe interference. This is caused by the very high temperatures created behind the shock which in turn create high electron densities. Indications are that the electron density is homogeneous for some distance behind the shock before decaying to much lower values. The length of this region for the cases studied is given in Table 2. The one-way 10 GHz attenuation a normally incident* radar ray would experience through the first normal shock is listed below for the cases studied:

Table 3

N_a Impurity Level	VM-8	VM-10
System A		
1 PPM	1 db	12.5 db
10 PPM	2 db	54.6 db
System B		
3 PPM	$< 10^{-5}$ db	$< 10^{-4}$ db

The above results indicate the possibility of severe interference for the System A RADVS, whereas System B is essentially unattenuated. Significant refraction and phase shift will also occur with System A, but, as with attenuation, System B suffers negligible effects.

Shock reflection, although small in power, is important since it represents a possible path for transmitter to receiver leakage. RADVS is a CW doppler radar, which, by definition, has its receiver on simultaneous with the transmitter. Plume created leakage has the effect of raising the overall noise level of the receiver as the noise component of the reflection falls into the doppler band. Hence the receiver's sensitivity is decreased and the RADVS range shortened. Appendix A details the mechanism of normal shock leakage.

For the least interfering condition of System A, i.e., 1 db of attenuation, the noise leakage will be in the order of -50 db below the transmitted power level in the worst case. Since the RADVS receiver sensitivity is in the order of -150 db shock reflections severely limit the system even when the other shock effects are tolerable. This is also apparent with System B. Although all other interference effects are negligible, shock reflection is still significant. The principal reason for this is that, although the electron densities are very low, the neutral gas gradient across the shock front is quite large. This, coupled with the relatively high refractivity of the monopropellant exhaust gas (mostly NH_3), can produce leakage noise of about -122 db in the worst case.

B. Far Plume

This region, beyond all internal shocks, is characterized by having its pressure approximately that of the atmosphere it is exhausting into. A worst case analysis of plasma attenuation in this region indicates that the electron density is too low to cause any meaningful effect (i.e., attenuation less than 10^{-8} db/in). This also indicates that phase shift and refraction will be negligible. Reflections are insignificant because of the absence of sharp gradients.

C. Inviscid Core and Mixing Layer

This region is characterized as an underdense plasma devoid of meaningful gradients except along the oblique shock and the air-mixing layer boundary. These gradients are not as severe as the normal shock nor are the gas and electron densities nearly as high as behind the normal shock. From these arguments, and assuming negligible turbulence backscatter, it is tacitly assumed that leakage from these boundaries is much less than that from the normal shock for any given set of conditions.

This region can produce serious attenuation and phase shift for System A. This is due to the possibility of very long electrical path lengths. Figure 7(a) shows a ray in the plane of the plume axis which is traveling parallel to the axis at 20 inches. This ray might be typical of the 0 db ray of an altimeter beam. For the path shown (1 to 2) the attenuation is 2.0 db, one way. The total relative phase shift along this path is about 535 degrees. This calculation assumes 10 PPM impurity and is a worst case situation for this particular ray.

There will be no significant attenuation in this regime for System B.

V. System Optimization

It is clear from Section IV that the normal shock regions should be avoided for both systems (but in particular System A). Based upon the methods of Section III, the region containing all the expected shocks under all thrust conditions can be described geometrically.

In Figure 7(b) the conical region from the nozzle is an approximation of the curve in Figure 4(b) which describes all first normal shocks;

*The amount of attenuation increases with path length which increases for oblique incidence. Although normal incidence is non-typical, it is a minimum value for reference purposes.

the inverse cone in dotted lines from the first normal shock at full thrust bounds additional normal shocks; and the cylinder indicates possible regions of high electron concentrations resulting from normal shocks.

RADVS beam avoidance of this cone-cylinder region in System B should eliminate all interference-leakage effects. This is not the case in System A as attenuation and phase shift can still occur outside the shock as pointed out in Section IV-C.

If shock region avoidance is not possible, then the shock interference contribution can be determined in the manner described in Section III-C. The intermediate field, between shocks, is not well known and interference calculations can not be more than rough estimates.

The contribution from the shock region (if any) can be added directly to the contributions from the rest of the plume. The other contributions, in general, require detailed knowledge of the ray path. This requires the calculation of a skew ray traversing an axisymmetric, three-dimensionally inhomogeneous, refracting medium. Outside of the normal shock zone refraction is small due to the well-underdense nature of the plasma. For ease of calculation, it is reasonable to ignore this small refraction when determining ray paths.

With this approximation the partial interference is determined for a candidate RADVS arrangement for System A where optimum normal shock avoidance by the 4 active beams is accomplished. The details of this analysis are given in Appendix B. For the worst case (the largest plume) the most severe interference was 0.07 db one-way attenuation for the 0 db ray, and 0.55 db for the 3 db ray of the No. 3 doppler beam. (See Figure 7(a).) This interference may be tolerable, but it certainly is not negligible, particularly when it is remembered that upon this steady state attenuation is a noise perturbation which will degrade the system in its own right.

It is important to note that the hypothetical ray calculated in Section III-C experienced considerably more attenuation than the above rays even though the path over which it was calculated is shorter. This comparison points up the importance of determining in detail through what region of the inhomogeneous plume the RADVS beams pass. Each particular beam-plume geometry is different and scaling from one to another could be very misleading. Each candidate geometry should be assessed individually.

VI. Conclusions

This preliminary analysis indicates clearly that interference caused by the internal shocks can be critical. The general character of the interaction can be determined, however, so that the problem can be negated to a large extent by geometrical considerations in the design of the system. Since for certain systems (such as A) it may not be possible to eliminate interference by beam-plume positioning, an overall assessment of the problems of a partially interfering plume has been made. By the analysis methods described in this paper, it is possible to optimize the geometrical layout of any candidate Voyager RADVS system with regard to plume interference.

Appendix A

Normal Shock Reflected Noise

Reflections off of the plume can occur in two ways:* turbulent backscatter and/or shock reflections. Of the two, the most significant for Voyager RADVS applications appears to be the latter. This is primarily due to existence of large normal shocks quite close to the vehicle. These shocks exist perpendicular to the thrust axis within the core of the plume. Up to four and more of these shocks can be present, regularly spaced along the plume axis. Their size and spacing depend primarily upon the ratio of nozzle emit pressure to ambient pressure. For very low ambient pressure, the normal shock is very far from the nozzle, and pressure and density behind the shock are very low. As the atmospheric pressure is increased (or the chamber pressure reduced, as, for example, to reduce thrust), the shocks get smaller and closer to the nozzle. Eventually the normal shocks disappear. Shock diamonds, familiar on boosters, occur for ambient pressure greater than nozzle exit pressure, and are composed only of the less intense oblique shocks. Due to the small normal shock sizes, reflections from boosters at low altitude are probably negligible.

Shock reflection, as with all other plume interference mechanisms, is comprised of a steady state component and a noise component. The relative magnitude of these components is a function of the intensity of local turbulence. Their absolute magnitudes are equally dependent upon the local electron density or neutral gas density (when electron levels are low).

The following discussion will consider the latter situation when the electron density is small and neutral gas effects dominate as in the case of System B.

Turbulent Gas Modulated Reflections

The noise modulation of the reflected signal is due primarily to the random variation of the index of refraction behind the normal shock. Other effects include the varying index in front of the shock, the varying roughness character of the shock and the variation in shock location due to engine combustion instabilities. These latter effects are insignificant in the Voyager problem. The refractivity behind the shock is 7.5 times that in front, so the effects in front can be considered second order. Due to high plume velocity, it is estimated that the shock roughness will be less than 1/10 of a wavelength at the RADVS frequency and it, too, is probably second order. Finally, any engine instability

*Providing that the plume plasma is underdense. All proposed RADVS applications to date have met this criteria.

is probably below 1 percent of the thrust level and would not cause a significant shock movement. Even if it were higher, the interference would be coherent in nature rather than noise and could hopefully be dealt with by selective filtering.

Noise variations in the refractive index of a gas caused by turbulence has been studied for years by radio scientists. Their primary concern to date has been tropospheric propagation with little regard to rocket exhausts. The only analytical work on the exhaust problem was done in 1965 by Geiger.[9] He applied the theory of Booker and Gordon,[10] the accepted theory of troposcatter to forward scatter telemetry through booster plumes. Recently, Smoot and Seliga[11] compared Geiger's theory to their experimental data on small solid fuel plumes. Their results had poor agreements with theory. In applying the theory they used turbulence data taken on a small subsonic jet by Gultract, et al.[12] Application of this data to rocket plumes is questionable. Unfortunately, there was no alternative since rocket exhaust turbulence measurements have not been made to date. Because of this, Smoot and Seliga could not definitely establish the validity of Geiger's theory. To the authors' knowledge, no other theoretical work or meaningful experimental work had been done on plume noise. Geiger's theory cannot be applied to normal reflections since it deals only with single scattering in the forward direction. Plane reflections are different mechanisms requiring the use of the Fresnel reflection theory. From it, for normal incidence, the reflection coefficient is,

$$R = \frac{N_2 - N_1}{2} \qquad \text{(A1)}$$

where N_1 and N_2 are the refractivity of the gases in front of and behind the normal shock. The refractivity is defined as

$$N = n - 1 \qquad \text{(A2)}$$

where n is the index of refraction.

Since across the shock $N_2 = 7.5\ N_1$ we can let

$$R \cong \frac{N_2}{2} = \frac{N}{2} \qquad \text{(A3)}$$

If there is a noise perturbation on the refractivity due to turbulence we can write,

$$N = \bar{N} + \frac{1}{S}\int_S \delta N(t, r)\, ds \qquad \text{(A4)}$$

where S is the surface of the shock, $\bar{N}$ the average or steady state refractivity and $N(t, r)$ the turbulent perturbation.

Finding the reflection coefficient

$$R = \bar{R} + \delta R = \frac{1}{2}\left(\bar{N} + \frac{1}{S}\int_S \delta N(t, r)\, ds\right) \qquad \text{(A5)}$$

and equating the mean square of the perturbation terms, we have upon averaging over time

$$\overline{\delta R_p} = \overline{(\delta R)^2} = \frac{1}{4S^2}\,\overline{(\delta N)^2}\int_{S_1}\int_{S_2} f(r_1 - r_2)\, ds_1\, ds_2 \qquad \text{(A6)}$$

If it is assumed that the turbulence has the correlation function

$$f(r_1 - r_2) = e^{-r/a}$$

where a is the spatial scale of turbulence, then for R = shock radius we can write

$$\overline{\delta R_p} = \frac{1}{4S}\,\overline{(\delta N)^2}\int_{-\pi}^{\pi}\int_0^R r\, e^{-r/a}\, dr\, d\theta$$

$$= \frac{\pi a^2}{2S}\,\overline{(\delta N)^2}\left[1 - \left(\frac{R}{a} + 1\right) e^{-R/a}\right] \qquad \text{(A7)}$$

The turbulent intensity of the gas density (ρ) variations is defined as

$$I = \frac{\overline{(\delta\rho)^2}^{1/2}}{\bar{\rho}} \qquad \text{(A8)}$$

Since

$$N \propto \rho \qquad \text{(A9)}$$

we can write

$$\overline{\delta R_p} = \frac{\pi a^2}{2S} I^2 \bar{N}^2 \left[1 - \left(\frac{R}{a} + 1\right) e^{-R/a}\right] \qquad \text{(A10)}$$

Accurate estimates of I in rocket exhaust plumes are non-existent due to the absence of experimental data. The closest data is the subsonic jet of Reference 8. Their measured value of I is 0.5 along the jet core. Their measurements also indicate that a is in the order of the nozzle diameter and grows with distance downstream.

Therefore if we assume a = R then

$$\overline{\delta R_p} = \frac{0.266}{8}\,\overline{(N)^2} \qquad \text{(A11)}$$

is the mean value of the noise reflections.

$\bar{N}$ can be found from the Clausius-Mossotti equation which describes the dielectric constant of a gas.[13] For the monopropellant of System B the shock reflection is

$$\overline{R_p} = \frac{\overline{(N)^2}}{4} = -113 \text{ db} \qquad \text{(A12)}$$

therefore

$$\overline{\delta R_p} = -122 \text{ db} \qquad (A13)$$

This value is well above the noise of a typical RADVS receiver. For example, Surveyor's sensitivity is greater than -152 db,[14] so that the above shock reflection could in the worst case of normal incidence degrade receiver sensitivity by 31 db.

This analysis, although admittedly crude, clearly points up the possibility of normal shock leakage in a plume where ionization effects are negligible.

Appendix B

Calculation of Beam-Plume Interaction

It is customary in considering the interaction of an e.m. wave and a rocket exhaust plume to apply the geometric optics approximation. In the resulting theory, the RADVS beam can be considered as a bundle of independent rays. Since much of the plume interaction occurs in the antenna's near-field zone, it is further assumed that each ray emanates from a specific point in the aperture. For example, a -3 db ray is assumed to start from the aperture's edge while the 0 db ray comes from the center. The result is that the rays in the near field are all parallel, forming a cylinder whose diameter is the major dimension of the aperture. At the Rayleigh range the cylindrical beam geometry commences to expand as a cone whose angle is that of the beam-width. For the present Voyager RADVS concept the Rayleigh range is about 200 inches from the aperture.

The rays are all parallel to the beam pointing direction in the near field. This direction can be related to the vehicle's thrust axis by the angle, θ. The RADVS under consideration has $\theta = 20.6$ degrees for its velocity beams and $\theta = 0$ for the altimeter. If the descent engine points along the thrust axis, then the velocity beam rays also make a 20.6-degree angle with projections of the plumes' centerlines.

If the radar beams are positioned in order to miss the center shock region of the plume, then the beam rays and the plume axis do not lie in the same plane and are geometrically skewed. This is not true of the altimeter beam's near field, because, even though it avoids the plume core, its rays are always parallel to the z-axis.

Figure 8(a) shows the RADVS-plume geometry studied. (System A with a Surveyor type RADVS.) Pictured is the projection of the radar beams in the exit plane. Also pictured is maximum plume diameter at the normal shock. All three plumes lie parallel to the thrust axis except plume No. 4, which can be gimbaled ±12 degrees in the manner shown. This beam plume geometry yields the minimum interference consistent with the restraints of RADVS location. Assuming that beam No. 4 is a spare and the interference it has with the gimbaled engine can be tolerated, then the closest beam-plume combination appears to be beam No. 3 with plume No. 3.

Figure 8(b) is an exit plane projection showing the details of the beam No. 3-plume No. 3 interaction. Conveniently, the RADVS aperture lies on the exit plane so that a line can be drawn connecting the center of the plume with the center of the aperture. Assuming the origin of a cartesian coordinate system is the intersection of the plume's centerline (the plume is directed into the paper) and the exit plane (the plane of the paper), then the line can be considered as the y-axis. A right-hand coordinate system can then be constructed with the positive x-axis into the paper (along the plume).

The equations locating a skew ray in the coordinate system are

$$x = x_o + \rho \cos \alpha \qquad (B1)$$

$$y = y_o + \rho \cos \beta \qquad (B2)$$

$$z = \rho \cos \gamma \qquad (B3)$$

where x_o and y_o are the coordinates of the ray's intersection with the x - y plane, ρ is the distance from the intersection to the point and α, β and γ are the angles made with the lines parallel with the x, y, and z axes that pass through the points x_o and y_o. Cos α, cos β, and cos γ are simply the direction cosines of the ray.

A rocket exhaust plume is an axisymmetric structure which can be described in cylindrical coordinates, r and x. The x coordinate relates directly to the cartesian x while the r is given by

$$r = (y^2 + z^2)^{1/2} \qquad (B4)$$

Given the fact that the beam intersects the thrust axis at 20.6 degrees (α) and given an exit plane projection of the geometry (Figure 8(b)) then the addition ray parameters can be found. y_o is merely the distance from the intersection point to the origin as measured on Figure 8(b). Measuring the projection line "a" the x - y plane intersection coordinate x_o for the closest -3 db ray can be found by

$$x_o = \frac{a}{\tan^{-1} \theta} \qquad (B5)$$

The distance ρ' (see Figure 8(b) (insert)) is given by

$$\rho' = \frac{a}{\sin^{-1} \theta} \qquad (B6)$$

Letting $\rho' = \rho$ with $r = R$ (measured from Figure 8(b)) Equations (B2), (B3), and (B4) can be solved simultaneously along with the direction cosine relationship

$$\cos^2 \alpha + \cos^2 \beta + \cos^2 \gamma = 1 \qquad (B7)$$

to yield β and γ.

The preceding calculations yield the parameters describing the -3 db ray. The 0 db ray is parallel to it (in the near field) so that its direction cosines are the same, however, it originates on the y axis so its x_0 is equal to 0 and its y_0 is simply the distance to the origins as measured on Figure 8(b).

Figure 7(a) shows the two skew rays (-3 db and 0 db) projected into the axisymmetric plume coordinate system (r, x). This transformation is accomplished using Equations (1) – (4). The straight rays appear curved in this coordinate system because the distance r is the radial length from a point on the ray to the x-axis. The curved line has a minimum where the ray and the plume are in closest proximity. These examples are typical of all skewed rays which do not intersect the x-axis. For the special case, where it does, the ray will appear straight.

Figure 7(a) also shows a possible worst-case altimeter beam ray. This ray is a hypothetical example and is not a part of the installation in Figure 8. It is a non-skewed ray (as all altimeter beam rays are in the near field) located parallel and at a distance of 20 inches from the plume axis. It is highly instructive to compare this ray with the other two.

The attenuation along each ray was calculated using Equation (8). The one-way path attenuations for each ray are:

Case	Attenuation
Skewed ray (0 db)	0.072 db
Skewed ray (-3 db)	0.55 db
Straight ray	2.0 db (from 1 to 2)

As expected the -3 db skew ray suffers significantly more attenuation than the 0 db ray. Apparently this is only because it cuts more of the plume. However, the straight ray obviously has a shorter path (1 to 2), but undergoes 4 times the attenuation of the -3 db ray. This apparent contradiction is explained as follows. While having a much longer path, the -3 db ray passes through large distances of weak plasma, i.e., the mixing layer and inviscid core. It has relatively short path lengths through the denser shock regions. Conversely, the straight ray skims the oblique shock for a significant portion of its path. The plasma's electron density in this region is considerably larger than the adjacent regions (although not nearly as dense as the normal shock). The larger attenuation is a vivid example of the crucial dependence the path has upon propagation.

References

1. A. J. Kelly, "Analysis of the Interaction of the Surveyor Radar Altimeter Doppler Velocity Sensor System and Vernier Thrust Chamber Plumes," JPL TR32-927, April 1966.

2. "T-2N Surveyor Test Vehicle Tether and Descent Test Series," Final Rept. JPL Contract No. 950056, Hughes Aircraft Company, July 1966.

3. W. J. Miller and H. S. Pergament, "Radar Interference Effects in the LEM Descent Engine Exhaust Plume," AeroChem TP-118, July 1965.

4. C. H. Lewis, Jr. and D. J. Carlson, "Normal Shock Location in Underexpanded Gas and Gas-Particle Jets," AIAA J. Vol. 2, No. 4, p. 776, April 1964.

5. P. Molmud, "The Electrical Conductivity of Weakly Ionized Gases," ARS Ions in Flames and Rocket Exhausts Conference, October 1962, ARS Reprint 2586-62.

6. J. G. Seubold, "Turbulent Mixing of a Two-Dimensional Free Jet," AIAA Paper 65-821, December 1965; reprinted as Hughes Aircraft Company Aerospace Technology Research Rept. 10.

7. L. D. Smoot, D. L. Underwood, and R. G. Schroeder, "Prediction of Microwave Attenuation Characteristics of Rocket Exhausts," March 1966, J. of Spacecraft and Rockets, p. 302.

8. J. W. Shirie and J. G. Seubold, "Length of the Supersonic Core in High-Speed Jets," AIAA J., November 1967, p. 2062.

9. A. A. Geiger, "Analysis of the Effects of Rocket Exhaust Fluctuations on FSK Telemetry," AIAA 6th Solid Propellant Rocket Conference, Washington, D.C., February 1-3, 1965, AIAA Paper No. 65-184.

10. H. G. Booker and W. E. Gordon, "A Theory of Radio Scattering in the Troposphere," Proc. of IRE, April 1950, p. 401.

11. L. D. Smoot and T. V. Seliga, Jr., Rocket Exhaust Plume Radar Attenuation and Amplitude/Phase Noise, J. of Spacecraft and Rockets, Vol. 4, June 1967.

12. H. Guthart, D. E. Weissman, and H. Morita, Diagnostics and Microwave Scattering for an Underdense Turbulent Plasma, Stanford Research Institute, Tech. Rept. 27, May 1965.

13. R. S. Elliot, "Electromagnetics," McGraw Hill Pub. Co., New York, N. Y., 1966, p. 366.

14. Research Triangle Institute, "Surveyor Landing Radar Test Program Review," Final Rept., JPL Contract No. 451603, January 24, 1967.

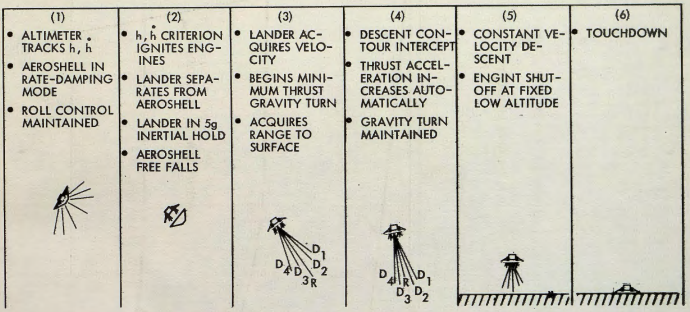

FIGURE 1a VOYAGER DESCENT (D_1 - D_4 AND R DEPICT THE 4 BEAM RADVS)

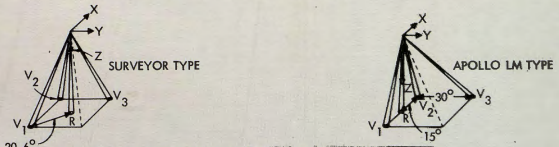

FIGURE 1b BEAM ARRANGEMENT OF CANDIDATE RADVS SYSTEMS

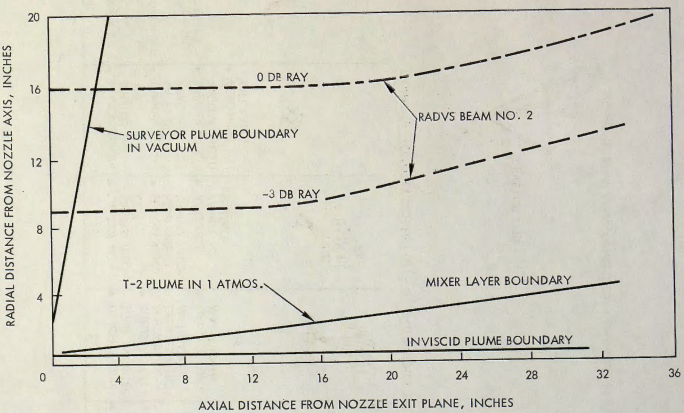

FIGURE 2
SURVEYOR SPACECRAFT AND T-2 TEST VEHICLE INTERFACE GEOMETRY OF RADVS BEAM NO. 2 WITH VERNIER ENGINE NO. 1 PLUME.

VERNIER ENGINE NO. 1 GIMBALED TO A MAXIMUM 5.5° TOWARD DOPPLER BEAM NO. 2

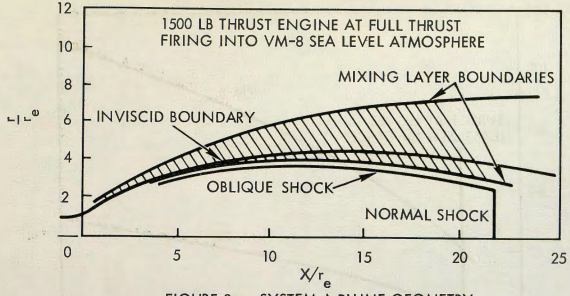

FIGURE 3a SYSTEM A PLUME GEOMETRY

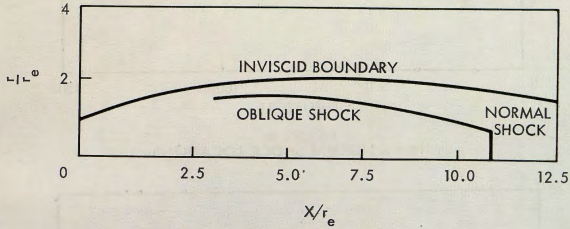

FIGURE 3b
SYSTEM A PLUME GEOMETRY 1500 LB THRUST ENGINE AT FULL THRUST FIRING INTO VM-10 SEA LEVEL ATMOSPHERE

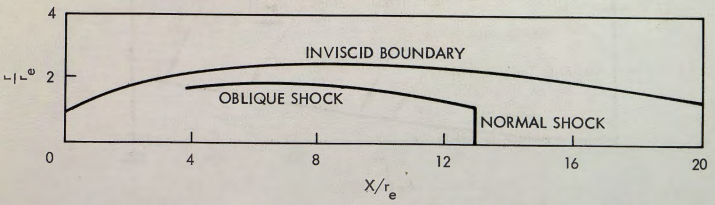

FIGURE 3c
SYSTEM B PLUME GEOMETRY 1000 LB THRUST ENGINE AT FULL THRUST FIRING INTO VM-8 SEA LEVEL ATMOSPHERE

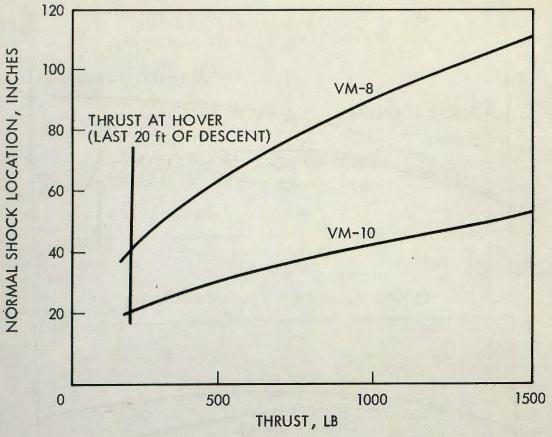

FIGURE 4a
SYSTEM A NORMAL SHOCK LOCATIONS

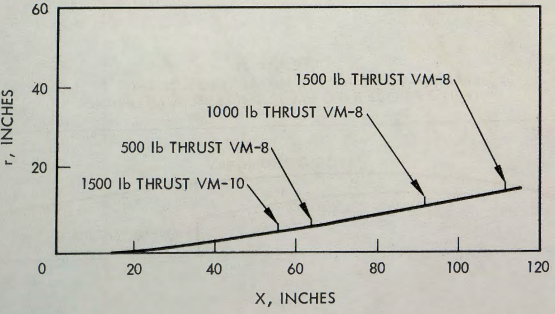

FIGURE 4b
SYSTEM A NORMAL SHOCK BOUNDARY
VARIATION WITH THRUST AND ATMOSPHERIC MODEL

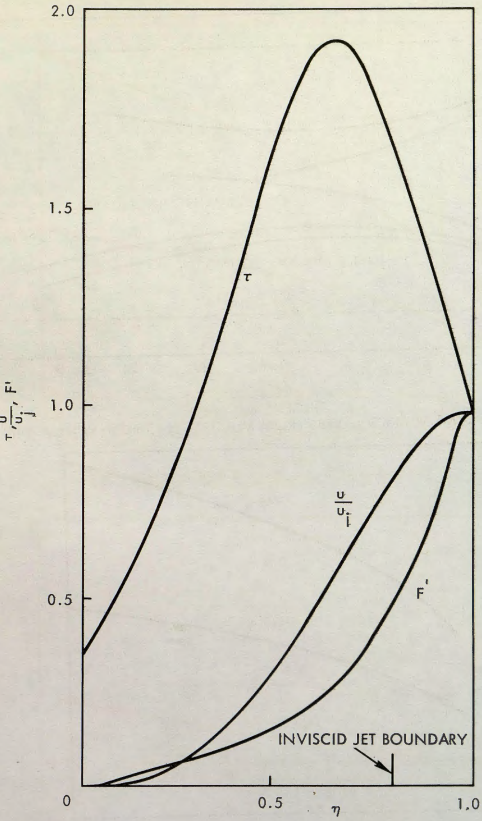

FIGURE 5
SYSTEM A MIXING LAYER CHARACTERISTICS IN VM-8 ATMOSPHERE

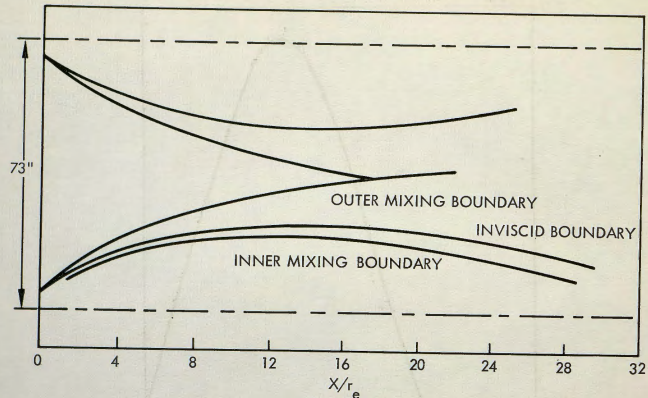

FIGURE 6a
COALESCENCE OF PLUME MIXING LAYERS FROM MULTIPLE ENGINES (SYSTEM A IN VM-8)

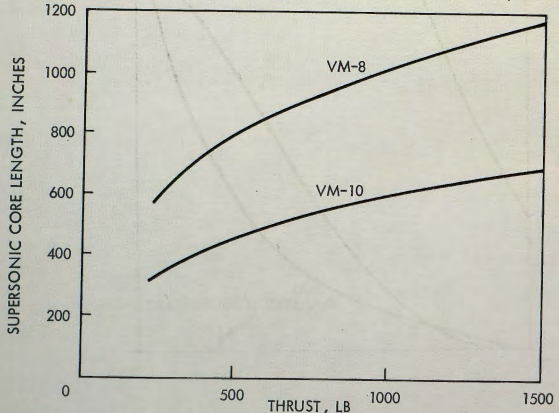

FIGURE 6b
SYSTEM A SUPERSONIC CORE LENGTHS

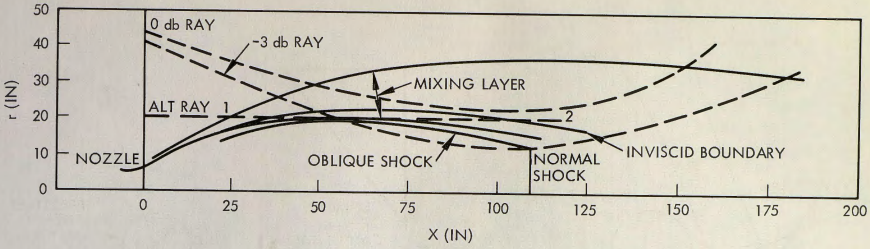

FIGURE 7a
RAY PATH OF A SKEWED DOPPLER BEAM AND A "STRAIGHT" ALTIMETER BEAM
IN THE CYLINDRICAL COORDINATE SYSTEM OF THE PLUME (SYSTEM A IN VM-8)

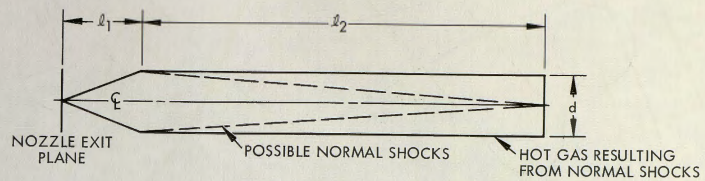

	SYSTEM A VM-8	SYSTEM A VM-10	SYSTEM B VM-10
d	27"	8.2"	10"
ℓ_1	111"	55"	55"
ℓ_2	490"	240"	240"

FIGURE 7b
NORMAL SHOCK AVOIDANCE REGION

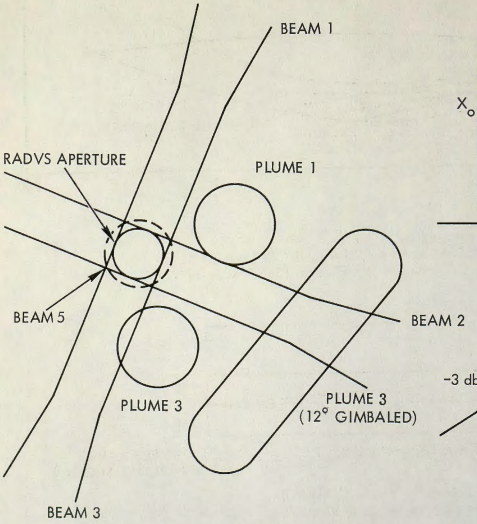

FIGURE 8a
EXIT PLANE PROJECTION OF VOYAGER BEAM-PLUME INTERACTION (SYSTEM A WITH SURVEYOR TYPE RADVS)

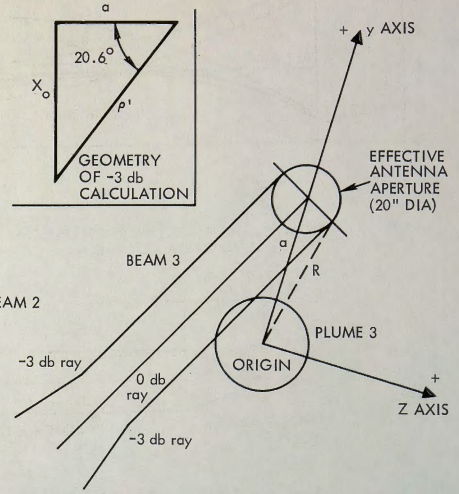

FIGURE 8b
INTERACTION GEOMETRY
BEAM NO. 3 - PLUME NO. 3